JKR Studies of Acrylic Elastomer Adhesion to Glassy Polymer Substrates

Dongchan Ahn[†] and Kenneth R. Shull[*,‡]

Department of Chemical Engineering and Department of Materials Science and Engineering, Northwestern University, 2225 North Campus Drive, Evanston, Illinois 60208

Received December 21, 1995[⊗]

ABSTRACT: Adhesion between a model acrylic elastomer and a glassy polymeric substrate has been investigated by the JKR technique. Hemispherical lenses of lightly cross-linked poly(*n*-butyl acrylate) (PNBA) were subjected to loading/unloading cycles on flat poly(methyl methacrylate) (PMMA) substrates. Significant adhesion hysteresis is observed at all accessible rates of unloading. The amount of hysteresis is seen to increase systematically with unloading rate and is characterized by the measured energy release rate (G). The presence of free PNBA chains, whether in the elastomer or applied directly to the interface, significantly reduces adhesion of the elastomer to the glassy substrate. Unloading profiles of the crack growth rate dependence of G yield a threshold value ($G(0) = 70 \pm 30$ mJ/m^2) which is close to the expected thermodynamic work of adhesion (W) between PNBA and PMMA. However, fits of the JKR model to loading data result in values of G which are significantly lower than W. We also examine the underlying assumptions of JKR analysis of fracture and test them by independent measurements of lens displacement (δ). The total energy dissipation in a hysteresis cycle is shown to be predicted accurately by JKR theory. Discrepancies between measured and predicted δ profiles are consistent with the effects of the finite thickness of the lens, which is not taken into account by JKR theory.

1. Introduction

Acrylic elastomers are widely used in coating applications because of their inherent thermal stability, oil resistance, and adhesive properties.[1] These same features make acrylic elastomers attractive for fundamental studies of polymer adhesion. This endeavor has been simplified recently by the development of techniques for producing monodisperse acrylic homopolymers and block copolymers from anionically synthesized parent polyacrylates,[2,3] thus allowing precise microstructural control of adhering surfaces. Unfortunately, typical adhesion measurement techniques such as peel tests or blister tests[4−8] offer limited sensitivity and are not well-suited for capitalizing on the "tunable interfaces" offered by monodisperse acrylic systems. These techniques may be used to measure an energy release rate (G), which can be viewed as the energy required to extend an interfacial crack by a unit area. Within the typical range of accessible crack growth rates, the G's obtained by such techniques at room temperature are usually orders of magnitude higher than the expected value of the thermodynamic work of adhesion (W), because the measurements are dominated by bulk viscoelastic energy losses incurred from deformation of the sample.[5,9]

An alternative adhesion test based upon the theory of Johnson, Kendall, and Roberts (JKR),[10] henceforth referred to as the JKR technique, has been used to probe the molecular causes of adhesion in a number of elastomeric systems. This technique minimizes the sample volume to reduce bulk viscoelastic losses, while maintaining much of the experimental practicality of the previously mentioned methods. Further, the JKR technique permits testing at a lower range of crack velocities where interfacial effects are unobscured by bulk effects. From early JKR experiments with natural and synthetic rubbers,[10−13] gelatin,[10] and polyurethanes[14,15] to more recent studies with poly(dimethylsiloxane) (PDMS)[13,16−19] and polyisoprene (PI)[20,21] elastomers, the usefulness and potential of this technique have been well established. However, there remain some poorly understood and/or conflicting results that need to be resolved in order to utilize the JKR experiment more effectively as a molecular probe of adhesion. The purpose of our work in this area is to shed new light on these questions and on more general questions relating to elastomer adhesion, by introducing to the literature a system based upon monodisperse polyacrylates that offers both industrial relevance and molecular control of interfacial structure. In this paper, we report the results of JKR adhesion tests between poly(*n*-butyl acrylate) (PNBA) elastomers and poly(methyl methacrylate) (PMMA). The latter is employed as a control substrate because its inertness and low surface energy (relative to metallic or silicon-based surfaces) are conducive to the creation of reproducible solid surfaces.

The validity of JKR theory in describing the adhesive contact of elastomers has been analyzed and discussed in detail by previous authors.[10,11,14,22−26] In brief, the radius of the circular contact area between two spheres pressed together by a load P is given by

$$a^3 = \frac{R}{K}\{P + 3\pi GR + [6\pi GRP + (3\pi GR)^2]^{1/2}\} \quad (1)$$

where a is the contact radius, G is the energy release rate, and R and K are effective radii of curvature and elastic constants, respectively, given by the following:

$$\frac{1}{R} = \frac{1}{R_1} + \frac{1}{R_2}$$

$$\frac{1}{K} = \frac{3}{4}\left(\frac{1-\nu_1^2}{E_1} + \frac{1-\nu_2^2}{E_2}\right)$$

Here, R_1 and R_2 are the radii of curvature of the spheres, ν_1 and ν_2 are their Poisson's ratios, and E_1 and E_2 are their Young's moduli. For the geometry of an elasto-

* To whom correspondence should be addressed. E-mail: k-shull@nwu.edu.
† Department of Chemical Engineering.
‡ Department of Materials Science and Engineering.
⊗ Abstract published in *Advance ACS Abstracts,* May 1, 1996.

S0024-9297(95)01892-4 CCC: $12.00

meric sphere ($\nu_1 = 0.5$) touching a hard ($E_2 \gg E_1$) and flat ($R_2 \rightarrow \infty$) surface, R reduces to the radius of curvature of the sphere, and K becomes equal to $^{16}/_{9}E$ of the sphere. (This geometry is of particular interest because it lends itself especially well to surface modification of the substrate.)[16,17,20,21,27] Inverting eq 1 yields the following expression for G explicitly:

$$G = \frac{1}{6\pi K a^3}\left[\frac{Ka^3}{R} - P\right]^2 \tag{2}$$

Thus, G may be obtained by monitoring the contact radius as a function of the applied load, provided R and K are known. We note that the original JKR derivation uses W in place of G in eqs 1 and 2; however, this original expression holds true only when the thermodynamic equilibrium conditions established by the initial contact of the two surfaces are sustained over the duration of the experiment. Maugis and Barquins[14] extended JKR theory to include nonequilibrium behavior by invoking linear elastic fracture mechanics arguments, yielding the form of the equations presented above.

It is common to observe significant hysteresis in the contact area profiles ($a^3(P)$) between application and subsequent release of the load. While the microscopic origins of this adhesive phenomenon are not fully understood, it has been attributed to processes such as interfacial diffusion of chains[28] or the formation of hydrogen bonds[18] between surfaces which alter the nature of the interface after contact, thereby giving rise to either an entirely new equilibrium or a kinetically trapped nonequilibrium condition. Also, viscoelastic energy losses on fracture will contribute to this hysteresis.[12] In general, the values of G obtained from equilibrium loading data (receding crack) will be less than or equal to W, whereas the G's resulting from unloading data (advancing crack) will exceed W, creating a driving force for extension of the crack until the equilibrium contact area is reached.

As in any fracture test of elastomer adhesion, implicit to the JKR analysis is a rate dependence of G during unloading. Quantification of such rate effects is desirable to experimentally test theoretical models of chain diffusion and pullout, for example. The variable used to characterize this rate dependence is the crack growth rate (v) which is given simply by the negative rate of change of a with respect to time ($-da/dt$). This rate dependence is often observed in peel tests of elastomers and has been related to a dimensionless viscoelastic energy dissipation function (Φ) by the following empirical expression[14,29,30]

$$G - W = W\Phi(a_T v) \tag{3}$$

where a_T is the well-known Williams−Landel−Ferry (WLF) shift factor.[31] The specific dependence of Φ on the reduced velocity, $a_T v$, appears to differ between various systems and regimes of study, but usually is reported in a power law fashion with an exponent between 0.6[14,32] and 1.[21] Exceptions to this behavior are found in the PDMS systems which exhibit considerably lower adhesion than do the more conventional organic backbone based elastomers. Silberzan et al.[18] observed no rate dependence in self-adhesion of PDMS and instead attributed the variation of G during unloading to the initial contact pressure, which depends upon location within the contact region according to JKR theory. It was argued that this P dependence arose from a pressure-sensitive chemical reaction at the interface. In contrast, Deruelle et al.[27] observed a power law type rate dependence of G in PDMS networks.

Despite such seemingly contradictory results from JKR fracture experiments, the PDMS systems do offer the advantage of allowing relatively accurate measurements of W (within 10%) from JKR loading curves, indicating that near-equilibrium conditions can be achieved. With PI elastomers, however, recent experiments by Creton et al.[21] for PI hemispheres on rigid flat PS substrates show that their value of G at zero load for a receding crack is somewhat less than the expected W.

In the following section, we present the physical details of our experimental technique. Section 3 contains the results of our JKR adhesion tests with PNBA lenses before and after extraction of the sol fraction, assuming the validity of JKR theory. Further discussion of these results with respect to existing literature follows in section 4. As will be seen, the G's obtained by JKR adhesion tests (on loading) of PNBA networks on PMMA are below the thermodynamic values. In order to determine the cause of this behavior and the other effects described above, section 5 re-examines the fundamental assumptions of JKR theory. Independent measurements of lens displacement are used to test these assumptions. Conclusions from this work are presented in section 6.

2. Experimental Section

JKR Apparatus. While instruments similar in spirit have been used to perform JKR experiments, our apparatus and experimental protocol are sufficiently different from those of prior experiments to merit a particularly thorough description here. The JKR apparatus is shown schematically in Figure 1a. Loading and unloading are controlled by a Burleigh Inchworm stepping motor and measured with a Schaevitz 50 g load transducer. The motor is manipulated by a series of digital pulses, each of which corresponds to a step of 5.5 ± 0.2 nm. The digital signal is sent either from a manual handset or from a desktop computer equipped with a National Instruments Lab PC+ data acquisition board and software interface (LabVIEW for Windows). Use of the computer-controlled interface enables precise control of both the rate and displacement of the motor shaft. The maximum velocity attainable with this motor is approximately 2 mm/min, while the minimum velocity is virtually unlimited. Concerns regarding the possible effects of torsion on the load measured by the linear variable differential transformer have been alleviated by calibrations with standard weights which show the load−voltage curve to be linear throughout the loading range of interest.

An Olympus BHMJL reflected light optical microscope with a 2.5× objective lens is used to observe the contact area through the transparent elastomer lens. Images are captured by a video camera and can be imported directly into a computer image analysis program (Image Pro Plus by Media Cybernetics) or recorded with a video cassette recorder with the time and load (in volts) digitally overstamped. The microscope base rests on an electronically modulated vibration isolation table (JRS Scientific) that reduces the noise level to below ± 0.05 mN. By isolating the instrument from air currents, the sensitivity may be improved further; however, dynamic experiments are currently limited to ± 0.10 mN by the resolution of the voltage reading that is stamped onto the video image.

The elastomer lens is attached directly to the bottom of a glass microscope slide which acts as the loading beam. It is then located within the field of view of the objective lens and centered over an optically smooth area of the substrate. Since the lens may leave behind some residue, any subsequent experiments involving the same substrate are performed on a previously unused portion of the surface. The substrate is held

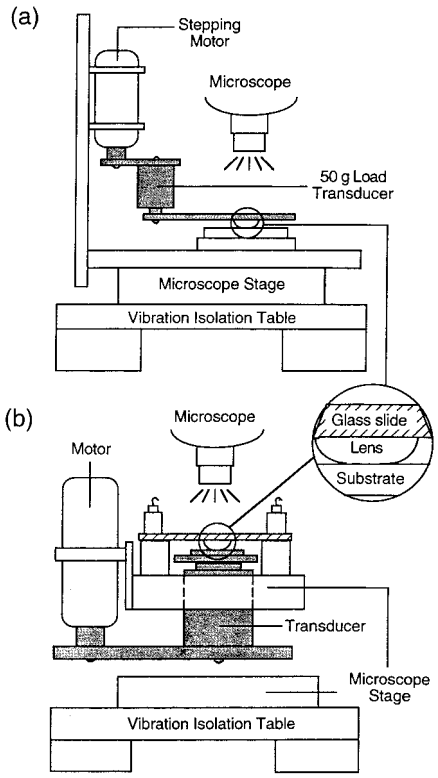

Figure 1. Schematic diagrams of the apparatus for JKR adhesion studies, with elastomer lens and substrate shown in the inset. The contact area is viewed through the transparent glass slide and lens. Moving parts of the assembly are shaded in gray. (a) Standard geometry for adhesion measurements. (b) Inverted, axisymmetric geometry for measurements of δ. Here, the substrate is moved by the motor while the lens support remains fixed.

fixed on both sides by weights which prevent any vertical motion of the substrate during pull-off of the lens. Quasi-equilibrium loading experiments are conducted by increasing the load in set increments, waiting a set time for the load and contact area to cease changing within that given time, and then acquiring an image. Dynamic loading is performed by increasing the load at a constant motor velocity. The contact radii are measured with a circle fitting function in the ImagePro Plus software with a conservatively estimated uncertainty of $\pm 2.3\ \mu$m. Before unloading, the maximum load, P_{max}, of the loading experiment is maintained for a given contact time, t_c. The load is then removed by reversing the motor, and images are captured over time. In the experiments reported here, t_c is kept under 10 min. The unloading is performed at a similar motor shaft rate as loading, resulting in a load profile which decreases from P_{max} and eventually reaches negative values before the lens pulls off from the substrate.

Displacement of the lens is measured by mounting the transducer in an inverted configuration to center the load directly over the transducer axis as shown in Figure 1b. This ensures that the spring constant of the apparatus can be calibrated to determine the true indentation of the lens. As opposed to the standard loading geometry where the lens is the moving surface, the substrate is attached directly to the transducer head, and the lens is stationary. The glass slide to which the lens is attached is held fixed between two supporting Teflon blocks underneath and weights on each side of the top surface. The spring constant (k_{app}) of this apparatus has been measured as 1000 ± 50 N/m, which is somewhere in between "fixed grips" ($k_{app} \rightarrow \infty$) and fixed load ($k_{app} \rightarrow 0$) conditions. Because we do not rely on pull-off force measurements, which are stability dependent,[14] the exact loading condition is not critical to our analysis. Lastly, we note that all experiments are conducted in ambient conditions.

Synthesis and Modification of Acrylic Polymers. Poly(*n*-butyl acrylate) was derived from a poly(*tert*-butyl acrylate) (PTBA) parent polymer. The PTBA was synthesized by living anionic polymerization at −78 °C in tetrahydrofuran (THF) with an excess of lithium chloride, after the technique of Teyssie et al.[2,3] *sec*-Butyllithium was reacted with diphenylethylene to form the initiator. The number-average molecular weight (M_n) of the sample used in this study was 55 000, having been determined by gel permeation chromatography (GPC) in THF calibrated with polystyrene (PS) standards. Klein et al.[33] have shown that the weight-average molecular weight (M_w) of PTBA obtained by GPC in THF with PS calibration agrees with M_w determined by light scattering for M_w below 100 000. GPC traces also yielded a polydispersity index (M_w/M_n) of 1.06, confirming the monodispersity of the PTBA. The glassy PTBA was then converted to PNBA by acid-catalyzed transalcoholysis in *n*-butyl alcohol with *p*-toluenesulfonic acid as the catalyst. Proton nuclear magnetic resonance (^{1}H-NMR) spectroscopy (Gemini 300 MHz) of the PTBA showed a dominant peak at 1.43 ppm due to the resonance of nine equivalent methyl protons on the *tert*-butyl group. After transalcoholysis, this peak was no longer observable and was replaced by several new alkyl resonances originating from nonequivalent methyl and methylene group protons on the linear *n*-butyl chain. Further, differential scanning calorimetry (DSC) (Perkin-Elmer DSC 7) also confirmed that the conversion was virtually complete, as indicated by the change in the glass transition temperature (T_g) from +42 to −52 °C. We note that acrylic acid moieties can also be introduced during the transalcoholysis process.[2,3,34] However, the low T_g of our polymer and the absence of an observable carboxylic acid ^{1}H-NMR peak indicate that the fraction of these groups must be very low. For comparison, the T_g's of the *n*-butyl acrylate and acrylic acid homopolymers are −54 and +106 °C, respectively.

Preparation of Lenses. PNBA was cured with dicumyl peroxide to form smooth hemispherical lenses in a procedure fashioned after the method of Chaudhury et al.[16] Five to ten weight percent peroxide was mixed into approximately 50 wt % solutions of PNBA in THF and dropped onto a glass slide pretreated with a 10% solution of 1*H*,1*H*,2*H*,2*H*-perfluorodecyltrichlorosilane (PCR, Inc.) in hexane. This treatment lowered the surface energy of the glass and caused the polymer solution to bead up into a hemispherical shape. Curing took place in a sealed glass vessel which kept the lenses under a partial pressure of argon during heating at 150 °C. After curing, the lenses were dried in a vacuum oven to ensure that any remaining solvent or dicumyl peroxide was removed. The radius of curvature of each lens was measured from a video image of the lens profile. Typical values of R varied between 1.0 to 1.5 mm. Networks were characterized by JKR loading experiments, in which a nonlinear least squares fitting routine fitted eq 1 to plots of a^3 vs P with K and G as adjustable constant parameters. This technique has been shown to give elastic moduli in good agreement with equilibrium swelling experiments.[13,21] It is known that peroxide curing of polyacrylates is quite inefficient.[1] In certain experiments the sol fraction was extracted from the lens by rinsing overnight with *n*-butyl alcohol in a Soxhlet extraction apparatus. After extraction, the radius of curvature of the lenses was reduced significantly. Therefore, the new R was inserted into eqs 1 and 2 when K and G were determined for extracted lenses.

Preparation of Substrates. Glassy substrates were created by spin coating a dilute solution of PMMA (Polysciences ($M_n = 500\ 000$, $M_w/M_n = 1.09$)) in toluene onto a precleaned silicon (Si) wafer at 3000 rpm. This process yielded uniform thin films between 900 and 1000 Å thick, as measured with a Sopra Moss ES4G/OMA ellipsometer. Free PNBA chains were placed on the PMMA substrates by spinning films from dilute *n*-butyl alcohol solutions. Resulting films were uniform in color, optically smooth, and free of pinholes.

3. Results

JKR Adhesion Tests of Unextracted PNBA Networks. A typical dynamic loading/unloading cycle of a lightly cross-linked, unextracted PNBA lens on a PMMA substrate is shown in Figure 2 for a relatively slow

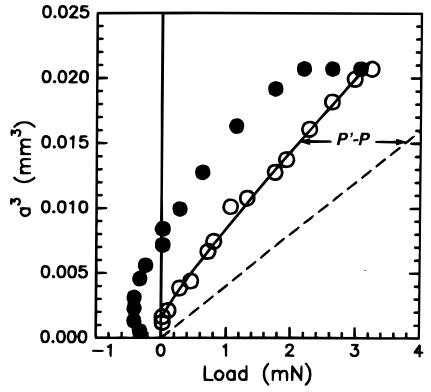

Figure 2. Typical JKR loading and unloading curves for an unextracted PNBA lens on a PMMA substrate. Data obtained on loading are depicted by open symbols, while unloading measurements are shown by filled symbols. The times required for loading and unloading were 430 and 540 s, respectively. Error bars in both a^3 and P are smaller than or equal to the symbol size. The solid line shows the best fit of eq 1, and the Hertz profile is shown by the dashed line.

loading rate of 8 μN/s. To relate the value of G to this plot, it is helpful to define an effective load, P', necessary to establish a contact radius of a in the absence of adhesive forces. Of course, in reality, the actual load P required to maintain the same contact radius is less than P' because the surface forces tend to enlarge the interfacial area. Therefore, when $G = 0$ in eq 1, then $P = P'$, and we recover the relationship between P' and a^3 for the contact of two elastic solids derived by Hertz[36] in 1880

$$P' = \frac{Ka^3}{R} \tag{4}$$

Referring back to eq 2, the bracketed term can now be rewritten as $(P' - P)^2$. This quantity is shown on Figure 2, and it follows that the square of this distance is proportional to G.

The most obvious feature of the data is the hysteresis between loading and unloading curves despite the glassy state of the PMMA substrate, which would not be expected to adhere particularly well to the PNBA. At a given contact radius, it is clear that G is considerably larger for unloading than for loading. It should also be noted that there is a difference between the times of unloading (t_u) (540 s) and loading (t_l) (430 s) that reflects the longer time required for the interface to break than to form. As noted by Silberzan et al.,[18] fitting unloading data with eq 1 results in artificially high values of K because of hysteresis. We therefore calculate G with eq 2 assuming a predetermined value of K obtained from the loading curves.

To examine the rate dependence of adhesion more precisely, it is necessary to relate G to the true interfacial crack velocity (v). Figure 3 reveals this relationship for the unloading data in Figure 2. The error bars in G were calculated from the standardized treatment of Kline and McClintock[37] in which the uncertainty in G, w_G, is given by

$$w_G = \left\{\left[\left(\frac{\partial G}{\partial R}\right)_{P,K,a} w_R\right]^2 + \left[\left(\frac{\partial G}{\partial a}\right)_{R,P,K} w_a\right]^2 + \left[\left(\frac{\partial G}{\partial P}\right)_{R,a,K} w_P\right]^2 + \left[\left(\frac{\partial G}{\partial K}\right)_{R,P,a} w_K\right]^2\right\}^{1/2} \tag{5}$$

where the w_i's denote the experimental uncertainty in the measurement of variable i. Based upon such factors

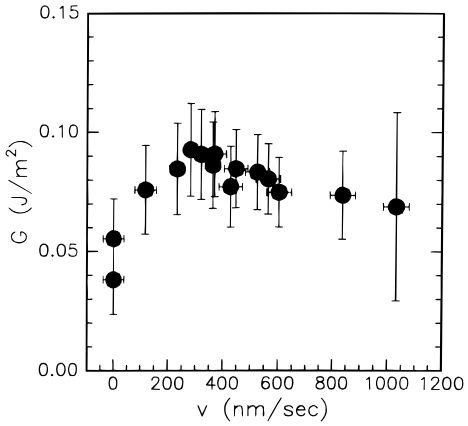

Figure 3. Dependence of G on crack growth rate for the unloading data shown in Figure 2. Vertical error bars were calculated from eq 5. Errors in velocity were obtained by combining the worst possible errors in measurements of a and t.

as noise in transducer voltage readings, video image resolution, and the possibility of improper fitting, the following values were assigned: $w_R = 0.025$ mm; $w_a = 2.3 \times 10^{-3}$ mm; $w_P = 0.09$ mN; $w_K = 0.03$ MPa. Partial derivatives were evaluated analytically from eq 2. Inclusion of the last term in eq 5 ensures a very conservative estimate of w_G, because K is not measured independently and is affected by uncertainties in the other variables. However, there is sufficient scatter in the K's obtained from various loading curves to merit incorporation of this uncertainty into our analysis. Horizontal error bars reflect the worst possible error in v based upon the uncertainties in a and t.

An important feature of Figure 3 is the critical value of G for the onset of observable crack growth, which we refer to as $G(0)$. Here, the value of $G(0)$ is within the range of the expected thermodynamic work of adhesion, estimated from available surface and interfacial tension data[35] to be approximately 70 mJ/m^2 for PNBA/PMMA. We also note the slight maximum in the curve, which we will discuss in greater detail later.

Figure 4 shows a series of experiments performed with the same lens and substrate at four different dynamic loading/unloading rates. Also shown are data from an experiment in which data were acquired in a step-by-step quasi-equilibrium manner. It can be seen that within experimental scatter, loading is independent of rate; however, the degree of hysteresis increases progressively with faster rates. Best fits of eq 1 to each of the loading experiments yields $K = 0.30 \pm 0.03$ MPa and $G = 25 \pm 10$ mJ/m^2. Assuming $K = 0.30$ MPa, we also have used eq 2 to determine G for each point on the loading curve. These calculations yield $10 < G < 40$ mJ/m^2, with the lowest values primarily corresponding to the lower range of loads ($P < 1$ mN). This effect is consistent with our observation from the quasi-equilibrium experiments that the contact area takes longer to cease increasing in this region of low loads. Further experiments performed by compressing a pair of PNBA lenses together (rather than in the lens-on-flat geometry) confirm that $G < W$ on loading, regardless of R or K of the substrate. Our results are in agreement with those of Creton et al., who observed similar phenomena with PI elastomers.[21]

Because two-parameter fits of eq 1 were used in the analysis of the loading curves, it is logical to question whether the surprisingly low values of G simply are a consequence of incorrectly low values of K, or vice versa. Therefore, we attempted to fit the data by fixing the

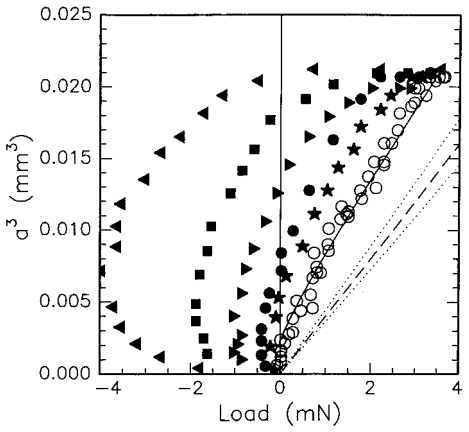

Figure 4. JKR loading and unloading cycles for the same unextracted PNBA lens and PMMA substrate used in Figure 2. The solid line is based upon the average values of K and G obtained from the best fits of eq 1 to all loading experiments ($K = 0.30$ MPa and $G = 25$ mJ/m^2). The dashed line represents the Hertz profile obtained from this average value of K. Dotted lines reflect the effect of uncertainty in K on the Hertz profile. Rates of unloading increase in succession from right to left. The quasi-equilibrium unloading experiment is shown by stars. Times of unloading are as follows: 4320 s (stars), 540 s (circles), 103 s (right-faced triangles), 43 s (squares), and 19 s (left-faced triangles).

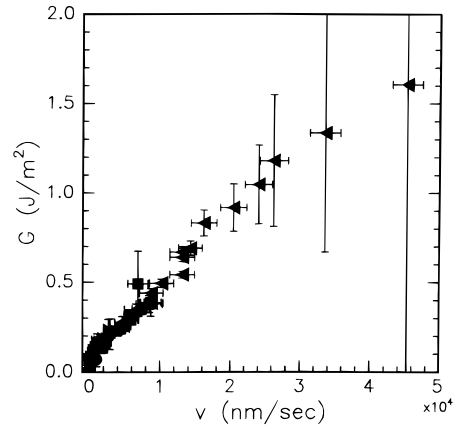

Figure 5. Master curve of crack velocity dependence of G for the unextracted PNBA lens on PMMA at all tested rates of dynamic unloading. The onset of crack growth is observed at $G(0) = 70 \pm 25$ mJ/m^2, close to the expected thermodynamic work of adhesion for PNBA−PMMA.

value of G at a more reasonable estimate of W (70 mJ/m^2) and varying K; however, this treatment resulted in unacceptably poor fits. From rubber elasticity theory,[31] the molecular weight between cross-links (M_{cl}) was obtained as 40 000 from the relationship $M_{cl} = 3\rho RT/E$, where R is the ideal gas constant (and not the lens radius of curvature). Considering that M_n of the PNBA prior to cross-linking is 55 000, this lens must be very lightly cross-linked. Extraction of the sol fraction was found to decrease the dry volume by approximately 10%, as determined by the 3.3% reduction in the lens radius of curvature. This result is reasonably consistent with the theoretical treatment of Charlesby[38] which predicts M_{cl} to be 35 000 for a network with 10 wt % sol fraction and starting molecular weight (M_{n0}) of 55 000, assuming a monodisperse starting polymer.

In keeping with Figure 3, a master curve of G(v) (Figure 5) obtained from the dynamic unloading data of Figure 4 yields a value of $G(0)$ that is much more representative of W. Also, the alignment of the data with v, which can be considered as a measure of an *interfacial* deformation rate, indicates that the rate of

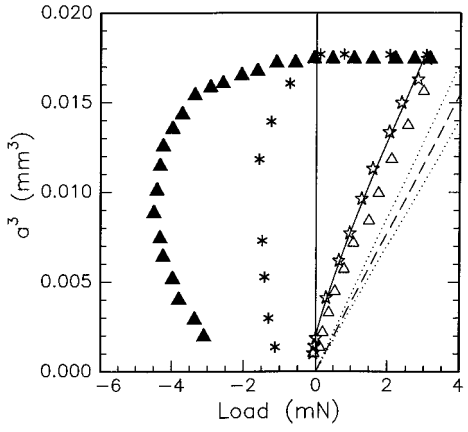

Figure 6. JKR loading/unloading cycles of the same PNBA lens after extraction of un-cross-linked PNBA chains. Note the change in scale from Figure 4 necessitated by the large increase in hysteresis. Open and filled triangles were obtained over times of loading ($t_l = 365$ s) and unloading ($t_u = 825$ s) which corresponds to rates similar to those used in Figures 2 and 3 (≈9 μN/s). Open stars represent quasi-equilibrium loading ($t_l = 4380$ s), and asterisks represent 11 h continuous dynamic release on unloading.

bulk sample deformation (given by the unloading rate) is not the determining factor in this range of v's. Rather, it appears that G is controlled largely by localized viscoelastic energy dissipation at the crack tip, as borne out by the agreement with the model of eq 3. Because all of the prior experiments were begun from nearly the same value of a_{max} with $P_{max} \approx 4$ mN, we also initiated unloading at the slowest rate (8 μN/s) from $P_{max} \approx 2$ mN and $P_{max} \approx 6$ mN to ensure that G(v) was not simply controlled by this particular value of P_{max} (or alternatively, a_{max}). These experiments yielded virtually identical values of G(v), so we can conclude that G(v) is independent of both the load and the location of the crack tip from which the unloading is commenced. (The same result was obtained for the extracted lenses described in the following section.)

JKR Adhesion Tests of Extracted PNBA Networks. Loading cycles on PMMA from experiments performed with the same lens after the sol fraction had been extracted are shown in Figure 6. The data exhibiting the most hysteresis (triangles) were obtained with a similar loading rate (9 μN/s) to that used for the data in Figures 2 and 3. Comparison of these points to Figure 2 reveals that extraction results in a significant increase in hysteresis. The other loading curve (stars) was obtained by quasi-equilibrium steps with approximately 6 min intervals between points. Its corresponding unloading curve was obtained in a continuous fashion, but a much slower descent in P was employed, with the entire experiment requiring 11 h from P_{max} until pull-off. Comparison with Figure 4 reveals that the unextracted lens requires unloading rates that are 3 orders of magnitude higher to attain the same amount of hysteresis, reflected in the most negative attainable load, that is exhibited after extraction. This dramatic increase in hysteresis is qualitatively similar to the behavior observed in studies of the self-adhesion of PDMS lenses.[18] Further, we observe a rate dependence on *loading* which was not evident when the sol fraction was present. Best fits of eq 1 to all loading curves still yield $K = 0.30 \pm 0.01$ MPa regardless of rate. The absence of the sol fraction therefore does not seem to affect the modulus significantly. However, loading rate does affect the magnitude of G, as indicated by the difference between values obtained from quasi-equilib-

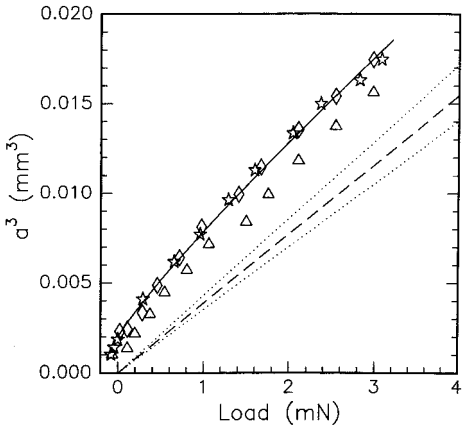

Figure 7. Loading data for the extracted PNBA lens on PMMA showing the rate dependence of crack recession. Triangles (t_l = 365 s) and stars (t_l = 4380 s) are the same as shown in Figure 6. Diamonds represent loading (t_l = 300 s) of the same extracted PNBA lens on a PMMA substrate coated with a 100 Å layer of monodisperse PNBA chains (M_n = 55 000) from which the lens was made. Note that despite the relatively fast loading rate, the presence of the free PNBA chains causes the contact radii to approach the quasi-equilibrium values on bare PMMA.

rium (G = 27.0 ± 3.2 mJ/m^2) and continuous slow loading (G = 11.5 ± 3.0 mJ/m^2). Removal of the sol fraction therefore appears to introduce a rate dependence of crack recession in addition to crack growth. Whether loading or unloading, the kinetics of the crack tip processes are retarded by extraction. The un-cross-linked PNBA chains in the lens must therefore act to lubricate the interface during crack recession and growth. If this picture were true, one would also expect that whether the free chains originated from the lens or the substrate, a qualitatively similar reduction in adhesion would be observed. To test this hypothesis, we spun cast a thin layer of free PNBA chains (100 ± 10 Å) directly onto the PMMA substrate. This PNBA was taken from the same batch (M_n = 55 000) from which the lenses were made. The resulting loading curve obtained with the extracted lens at the slow continuous rate of loading (10 μN/s) is shown in Figure 7. As expected, the dynamics of crack recession are now increased significantly, so that the contact areas approach those of the quasi-equilibrium curve. Curve fitting yields G = 21.8 ± 2.0 mJ/m^2 with K essentially unchanged (0.29 ± 0.01 MPa). This value of G, while still below the expected W, is closer to the value of G obtained from quasi-equilibrium data.

The lubricating effect of the free PNBA chains on unloading is also clearly seen in the G(v) plots of Figure 8. The data in part a were all obtained from similar unloading times. For the extracted lens on bare PMMA, G(0) = 150 ± 30 mJ/m^2. With free PNBA chains present, either in the lens or on the substrate, G(0) is reduced to near W. Since the threshold values of G are significantly different, we may conclude that the increase in adhesion of the extracted lens to bare PMMA is *not* simply a viscoelastic effect but is due to inherently different interfacial bonding mechanisms. Further, to ensure that this effect was not due to residual solvent trapped in the PMMA, we also attempted annealing the PMMA layer and repeating the measurement with the extracted lens. The ensuing value of G(0) was essentially unchanged from the unannealed PMMA case.

While G(0) is unaffected by whether the free chains are in the lens or on the substrate, it is somewhat

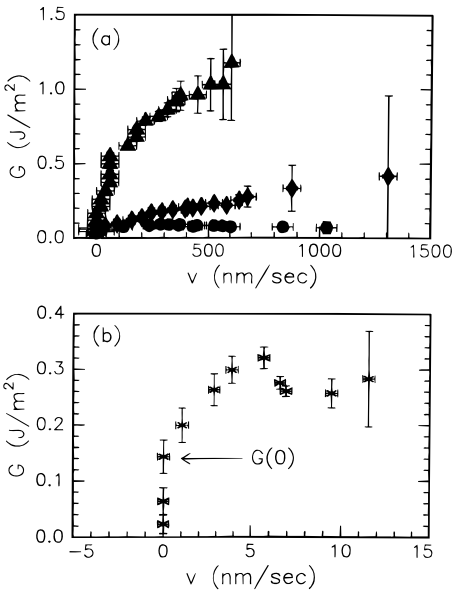

Figure 8. Lubrication effect of free PNBA chains on crack growth. (a) Data are shown for similar rates of unloading. Triangles represent the unloading of the extracted lens on bare PMMA (t_u = 825 s), diamonds show unloading of extracted lens on PMMA with a 100 Å overlayer of PNBA (t_u = 530 s), and circles represent unloading of unextracted lens on bare PMMA (t_u = 540 s). (b) Rate dependence of G from slowest (11 h) dynamic release of the extracted PNBA lens on bare PMMA. Note the increase in G(0) due to extraction of uncross-linked chains and the distinct maximum in G(v).

surprising that at any given finite v, G is lower when the lubrication originates from within the lens rather than from an interfacial layer. This result counterintuitively implies that the embedded sol molecules are more effective than the free PNBA chains applied directly to the interface. Such behavior could be explained by the presence of low molecular weight molecules in the sol. The presence of unreacted dicumyl peroxide may be ruled out because the lenses were dried *in vacuo* after curing at temperatures well above the decomposition temperature of the peroxide. Therefore, we tested whether our method of peroxide cross-linking of PNBA causes simultaneous chain degradation by soaking a lens in 1.5 mL of THF overnight to extract the sol fraction. Indeed, GPC analysis of the THF solution containing the PNBA sol showed a tenfold reduction in M_w and an increase in polydispersity index from 1.1 to 11.8. These low molecular weight PNBA chains should easily diffuse to the interface and would there act as much better lubricants than longer chains.

Because the 11 h release covers such a small range of velocities, it is shown separately on an expanded scale in Figure 8b. The G(0) obtained from this experiment is 140 ± 30 mJ/m^2. Similar to Figure 3, a maximum in G(v) appears in Figure 8b. Therefore, regardless of the interfacial kinetics, the maximum is observed when the unloading rate becomes sufficiently slow. Further experiments were conducted with two different lenses in the sphere−sphere geometry to ensure that the maximum in G(v) was not simply an artifact of this particular lens. These results confirmed the reproducibility of this effect.

4. Discussion of JKR Adhesion Tests

As noted by Shanahan and Carre,[32] formation of a new interface (crack recession or crack healing) may be described simply by a sign change on the left-hand side

of eq 3. In contrast to separation of an interface (crack growth), $W > G$ during loading, such that there is a resistance to crack growth, or a negative "crack growth motive" as coined by Maugis and Barquins.[14] The contact area will not equilibrate until $G = W$. The observed time dependence of loading associated with the extracted lens is therefore likely related to the viscoelastic dissipation processes that have been cited as the cause of adhesion hysteresis, contact angle hysteresis, and boundary friction.[28,39,40] However, the magnitude of the measured quantity $W - G$ is surprisingly high and suggests further examination to see whether the assumptions of JKR theory are met in our experiment.

On unloading, G significantly exceeds W and results in a positive driving force for the crack to grow at a velocity v. With unextracted lenses, $G(0)$ is close to the thermodynamic value as would be expected if the interfacial adhesion were simply due to attractive surface forces between PNBA and PMMA. The increase in $G(0)$ after removal of the free PNBA chains indicates that there is now an inherently stronger adhesive attraction between the network and the PMMA substrate. In light of the experiments of Ellul and Gent,[5] where the authors observed a significant increase in self-adhesion of polyisobutylene (PB) when free PB chains were added to the network, the large *reduction* in adhesion of PNBA to PMMA due to the presence of free chains may at first seem a bit surprising. However, in the case of Ellul and Gent, the increased self-adhesion was attributed to energy dissipated by pullout of the free chains after interfacial diffusion. Since PMMA is glassy and immiscible with PNBA, one would not expect interfacial diffusion to play a significant role in our control system. The low M_w of the free chains, particularly of the degraded sol fraction, virtually ensures that they are not entangled in the network. But with such slightly cross-linked networks, it may be possible for some slight interdigitation to occur just at the interface. Due to the nature of this curing scheme, it is difficult to characterize more definitively the structure of the network. Without further experiments, it can only be surmised that the free PNBA chains interfere with the mechanism that is responsible for strengthening the interface, be it physical (e.g., interdigitation) or chemical (e.g., hydrogen bonding between PMMA and PNBA). An alternative theory that evolves from theoretical treatments of chain pullout states that $G(0)$ should exceed W anyway because of the entropic penalty of chains exposed to the air.[41] In this case, $G(0) = 140$ mJ/m^2 may be closer to the true threshold value due simply to surface forces between the extracted network and PMMA. Then, the mobility of the free chains simply acts to reduce the measured G's by lubricating the interface[42] during dynamic crack growth and healing. Future experiments with anchored diblock PMMA−PNBA copolymer brushes should provide significant clues to the cause of this phenomenon.

The extrema in G(v) seen in Figures 3 and 8b are not predicted by eq 3 and to our knowledge have only been reported in cases in which the behavior is attributed to the glass transition of the elastomer[43] or to a change in the mode of failure from cohesive to interfacial failure.[44] These arguments fail to explain our data because G's are quite low and increase monotonically with crack velocity at higher unloading rates. Since the presence of a maximum in G depends upon the unloading rate rather than the interfacial velocity, it is likely a manifestation of underlying finite size effects which limit bulk viscoelastic dissipation or cause the JKR theory to break down in this limit. Analytical studies of viscoelastic deformation during fracture of finite sized double cantilever beam specimens predict such a maximum in G(v) which is not predicted for an infinite sized specimen.[45] Remembering that during the unloading experiment, v increases as the contact radius a decreases, the volume of the lens that is involved in dissipating energy must also shrink as the lens approaches pull-off. This situation is in contrast to peel experiments where the contact area remains relatively constant. However, this suppression of viscoelastic energy loss is countered by increasing v. For the finite volume effect to be observable, a obviously must be small, but additionally v also must be sufficiently low. This combination is apparently only met at the very lowest unloading rates we studied. As illustrated in Figure 9, it can be seen that as the rate of unloading is increased (t_u is shortened), v becomes progressively higher at any given a. An important implication of this result is that although the same lower range of v's is attainable even with higher unloading rates, the magnitude of the unloading rate does affect the sensitivity of the dynamic JKR unloading experiment. Though an a dependence of G is observed at very slow rates of unloading for small values of a, it differs from that observed in PDMS systems[18] in that our a dependence appears to result from geometrical confinement of the viscoelastic losses rather than to some underlying interfacial phenomenon.

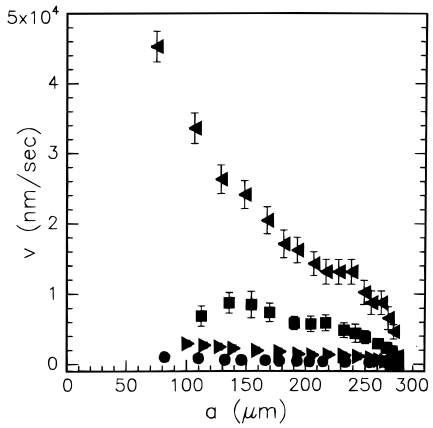

Figure 9. Relationship between v and a in the dynamic unloading experiments of Figure 4. Only the lowest unloading rate results in sufficiently low v at small a to allow the maximum in G(v) to be detectable.

5. Examination of JKR Theory by δ Measurements

In order to test the validity of the JKR analysis, we can measure the lens displacement δ independently using the axisymmetric experimental geometry shown in Figure 1b. These results are then compared to the displacements predicted by JKR theory (δ_{JKR}). Before presenting the analytical expression for δ_{JKR}, it is helpful to develop eqs 1 and 2 from basic fracture mechanics principles to examine the fundamental assumptions of JKR theory.

We begin with nonadhesive contact between two axisymmetrically aligned bodies. To achieve a given contact area A, we apply a load P' which results in a displacement δ'. The sign convention is such that compressive loads and displacements are positive. In

the presence of adhesive forces characterized by G, which act to increase the contact area, the load required to maintain the nonadhesive value of A will be less than P'. In order to maintain this original contact area, we must therefore reduce the load to a value $P < P'$ by applying an additional negative load, $P - P'$, which results in an additional negative displacement, $\delta - \delta'$.

Assuming linear elasticity, the standard generalized expression for G is given by

$$G = -\frac{P^2}{2}\frac{dC}{dA} \tag{6}$$

where C is the compliance ($C = \delta/P$).[46] For an axisymmetric system, $A = \pi a^2$. Here, eq 6 applies to the additional displacements and loads beyond those consistent with nonadhesive contact. Substituting $P - P'$ for P and $\delta - \delta'$ for δ gives

$$G = -\frac{(P' - P)^2}{4\pi a}\frac{dC'}{da}$$

$$C' = \frac{\delta - \delta'}{P - P'} \tag{7}$$

The quantity C' can be viewed as the compliance of the lens subject to the constraint of fixed contact area. Equation 7 is the most general relationship between G, P, δ, and a, provided that the system is linearly elastic. If δ', P', and the lens compliance are known, then measurements of P, δ, and a can unambiguously give a measure of G. In JKR theory, P' is given by eq 4, and δ' is related to a and R by the following expression:[10]

$$\delta' = \frac{a^2}{R} \tag{8}$$

The effective compliance, C', is given by

$$C' = \frac{2}{3Ka} \tag{9}$$

which when substituted into eq 7 along with the expressions for δ' and P' gives

$$\delta_{JKR} = \frac{a^2}{3R} + \frac{2P}{3Ka} \tag{10}$$

The basic assumption made by applying JKR analysis to calculate G is that displacements are elastic, i.e., that nonelastic behavior is limited to a small region near the crack tip.[47] Additionally, the expression for P' determined by Hertz[36] for spherical punches and generalized by Sneddon[48] for axisymmetric punches of arbitrary shape applies rigorously to the contact between a rigid punch on an elastic half-space. Recent numerical calculations by Ganghoffer and Gent[49] indicate that for rigid flat punches adhering to a flat elastic layer, the effective modulus of the elastic layer is determined by the ratio of the contact radius to the layer thickness. Though our experimental geometry is quite different, we may qualitatively surmise that the effects of the finite size of the lens may be manifest in differences between true and effective moduli. It is therefore also reasonable to question whether the lens thickness h (measured vertically from the base of the hemisphere to the center of the plane of contact) is sufficiently large relative to a and δ to be treated as an elastic half-space or if the approximation introduces significant errors.

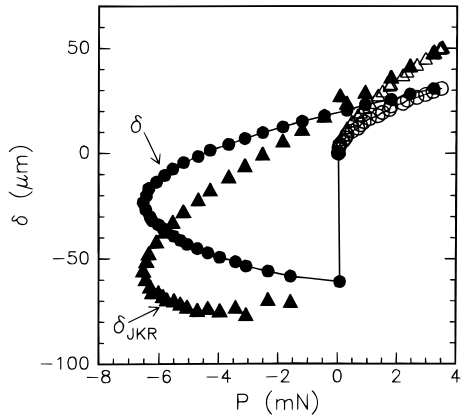

Figure 10. Comparison of measured δ (circles) with δ_{JKR} (triangles) calculated from eq 10 using simultaneously measured values of a. Open and filled symbols represent loading and unloading points, respectively. Data are shown for an extracted PNBA lens on a PMMA substrate. Note that the area enclosed by each hysteresis loop appears to be similar in magnitude. Measured values of δ are connected to guide the eye.

The proximity of a solid boundary can be expected to decrease the compliance of the lens in comparison to the JKR prediction. Alone, this consideration would cause the value of G obtained from JKR analysis to be somewhat higher than the actual value. However, the decreased lens compliance also would effectively increase K, thereby causing P' to exceed the JKR prediction. This effect works in the opposite direction, causing the JKR value of G to be less than the actual G. Because of the opposing influences of these deviations, it is possible that these effects can negate each other to give a reasonable predicted value of G, although, in general, the net effect of finite size on G is uncertain. It is readily apparent from inspection of eq 10, however, the finite size effects will result in $\delta_{JKR} > \delta$ for $P > 0$, and $\delta_{JKR} < \delta$ for $P < 0$.

Comparison with experiment (Figure 10) confirms that δ_{JKR} is indeed significantly higher than the measured δ at positive loads and lower than δ for $P < 0$. In all the experiments shown in this paper, the aspect ratio a/h varies between 0.5 and 0.6 at a_{max}. This value is almost assuredly too high to permit the approximation of the lens as an infinite half-space without introducing significant errors. Thus, we believe that the small size and bounded hemispherical shape of the lens are responsible for the mismatch between δ_{JKR} and δ. This result also supports our reasoning that finite size effects are responsible for the maxima that are observed in G(v) curves at low unloading rates. It is possible that nonlinear elastic effects also need to be taken into account, because of the relatively high strains associated with significant distortion of the lens.

A much better fit to much of the experimental curve (for $\delta > -25\ \mu$m) could be obtained by assuming a value of $K = 0.63$ MPa for the lens rather than the originally measured K. This value of K, however, appears to be artificially high because it yields values of G on loading which are a dependent and unreasonably exceed W at large a. Therefore, we may treat this value of K as a conservative upper bound on the true effective modulus of the lens. More reasonable values of G during loading are obtained by using $K = 0.40$. This value of K results in good agreement between $\delta(P)$ and $\delta_{JKR}(P)$ curves at low values of a, where finite size effects should not be as significant. Thus, the uncertainty in K ($w_K = 0.03$ MPa) employed in our error analysis in the preceding

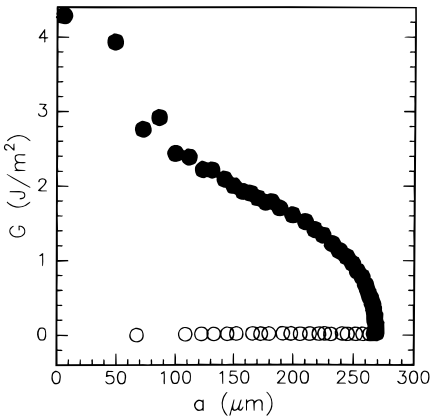

Figure 11. $G(a)$ curve obtained from JKR analysis of the experiment shown in Figure 10. This curve was used for integration to calculate U_{JKR}. Note that $G(a)$ is nearly constant during loading (open circles) and that values obtained during unloading (filled circles) greatly exceed those obtained during loading.

sections should partially account for these finite size effects.

In spite of the discrepancies between measured and predicted values of δ, the total areas within the theoretical and experimental $\delta(P)$ curves of Figure 10 are quite close. Since the curves are closed loops, the enclosed areas are a direct measure of the total energy dissipated (U) during the hysteresis loop as indicated by eq 11.

$$U = \oint P \, \mathrm{d}\delta = -\oint \delta \, \mathrm{d}P \tag{11}$$

From the concurrent JKR adhesion test, we numerically integrate the $G(a)$ curves to obtain the dissipated energy measured by JKR analysis (U_{JKR}) as shown in eq 12.

$$U_{JKR} = \int_0^{a_o} 2\pi a G(a)_{unload} \, \mathrm{d}a - \int_0^{a_o} 2\pi a G(a)_{load} \, \mathrm{d}a \tag{12}$$

As seen in Figure 11, $G(a)_{load}$ is nearly constant and much lower in magnitude than $G(a)_{unload}$; therefore, the integral is dominated by the data obtained during unloading. Calculation with eq 12 gives $U_{JKR} = 3.7 \times 10^{-7}$ J. Numerical integration of the area within the experimental $\delta(P)$ curve gives $U = 3.4 \times 10^{-7}$ J, which is in reasonable agreement considering the experimental uncertainty and systematic errors involved in the numerical integration. Our results indicate that in an average sense, different finite size effects do cancel one another out, resulting in a G which is reasonable, even though the JKR theory is no longer strictly valid in describing the specific $G(a)$ or $G(v)$ profiles. We further note that using $K = 0.63$ MPa to obtain an upper error limit in our calculations yields $U_{JKR} = 2.2 \times 10^{-7}$ J. This value is still within sufficiently reasonable agreement to validate our foregoing conclusions regarding the lubricating effect of free chains in the elastomer.

6. Conclusions

We have conducted studies of the adhesion between lightly cross-linked PNBA elastomer lenses and PMMA substrates by the JKR technique. A comprehensive and conservative analysis of experimental uncertainty has been conducted. The primary results that have emerged from this control study are as follows:

(1) Adhesion hysteresis is observed at all accessible rates of unloading for networks before and after the sol fraction is extracted. The amount of hysteresis increases systematically with the rate of unloading and is characterized by the measured energy release rate (G).

(2) The presence of free PNBA chains significantly reduces the adhesion of a cross-linked PNBA elastomer to a smooth PMMA substrate. This lubricating effect manifests itself in the following results:

(a) There is no apparent rate dependence on loading of unextracted PNBA networks on PMMA. However, after the sol fraction has been extracted, the kinetics of both interface formation and separation are noticeably slower and are rate dependent.

(b) The presence of free PNBA chains acts to reduce $G(0)$. From unloading of unextracted lenses, $G(0) = 70 \pm 30$ mJ/m^2 and is within the range of the expected thermodynamic work of adhesion for a PNBA−PMMA interface. Extracted lenses yield $G(0) = 130 \pm 30$ mJ/m^2. Further experiments with anchored PNBA−PMMA diblock copolymers on the substrate are being conducted to help determine whether the mobility of the free PNBA chains is giving rise to this lubrication effect.

(3) Measurements of lens displacement indicate that JKR analysis accurately predicts the total energy dissipation. Discrepancies between measured and predicted $\delta(P)$ curves are qualitatively consistent with the effects of the finite thickness of the lens, which are not taken into account by JKR theory. These finite size effects also explain the maxima observed in $G(v)$ at low rates of unloading. Inclusion of the uncertainty in K introduced by finite specimen size in our error analysis confirms that the results of our JKR adhesion studies are valid.

Acknowledgment. This work was supported by an NSF Young Investigator award, Grant No. DMR-9457923. Helpful conversations with Dr. C. Creton are also acknowledged.

References and Notes

(1) Starmer, P. H.; Wolf, F. R. In *Encyclopedia of Polymer Science and Engineering*; Mark, H. F., Bikales, N. M., Overberger, C. G., Menges, G., Kroschwitz, J. I., Eds.; Wiley: New York, 1985; p 306.
(2) Fayt, R.; Forte, R.; Jacobs, C.; Jerome, R.; Ouhadi, T.; Teyssie, P.; Varshney, S. K. *Macromolecules* **1987**, *20*, 1442.
(3) Varshney, S. K.; Jacobs, C.; Hautekeer, J.-P.; Bayard, P.; Jerome, R.; Fayt, R.; Teyssie, P. *Macromolecules* **1991**, *24*, 4997.
(4) Kinloch, A. J. *Adhesion and Adhesives*; Chapman and Hall: London, 1987.
(5) Ellul, M. D.; Gent, A. N. *J. Polym. Sci., Polym. Phys. Ed.* **1984**, *22*, 1953.
(6) Reichert, W. F.; Brown, H. R. *Polymer* **1993**, *34*, 2289.
(7) Gent, A. N.; Lewandowski, L. H. *J. Appl. Polym. Sci.* **1987**, *33*, 1567.
(8) Chu, W. Z.; Durning, C. J. *J. Appl. Polym. Sci.* **1992**, *45*, 1151.
(9) Ahagon, A.; Gent, A. N. *J. Polym. Sci., Polym. Phys. Ed.* **1975**, *13*, 1285.
(10) Johnson, K. L.; Kendall, K.; Roberts, A. D. *Proc. R. Soc. London A* **1971**, *324*, 301.
(11) Roberts, A. D.; Thomas, A. G. *Wear* **1975**, *33*, 45.
(12) Roberts, A. D. *Rubber Chem. Technol.* **1979**, *52*, 23.
(13) Vallat, M. F.; Ziegler, P.; Vondracek, P.; Schultz, J. *J. Adhes.* **1991**, *35*, 95.
(14) Maugis, D.; Barquins, M. *J. Phys. D: Appl. Phys.* **1978**, *11*, 1989.
(15) Rimai, D. S.; DeMejo, L. P.; Vreeland, W.; Bowen, R.; Gaboury, S. R.; Urban, M. W. *J. Appl. Phys.* **1992**, *71*, 2253.
(16) Chaudhury, M. K.; Whitesides, G. M. *Langmuir* **1991**, *7*, 1013.
(17) Chaudhury, M. K.; Whitesides, G. M. *Science* **1992**, *255*, 1230.

(18) Silberzan, P.; Perutz, S.; Kramer, E. J. *Langmuir* **1994**, *10*, 2466.
(19) Leger, L.; Hervet, H.; Marciano, Y.; Deruelle, M.; Massey, G. *Isr. J. Chem.* **1995**, *35*, 65.
(20) Brown, H. R. *Macromolecules* **1993**, *26*, 1666.
(21) Creton, C.; Brown, H. R.; Shull, K. R. *Macromolecules* **1994**, *27*, 3174.
(22) Maugis, D. *J. Colloid Interface Sci.* **1991**, *150*, 243.
(23) Tabor, D. *J. Colloid Interface Sci.* **1977**, *58*, 2.
(24) Derjaguin, B. V.; Muller, V. M.; Toporov, Y. P. *J. Colloid Interface Sci.* **1978**, *67*, 378.
(25) Muller, V. M.; Yushchenko, V. S.; Derjaguin, B. V. *J. Colloid Interface Sci.* **1980**, *77*, 91.
(26) Horn, R. G.; Israelachvili, J. N.; Pribac, F. *J. Colloid Interface Sci.* **1987**, *115*, 480.
(27) Deruelle, M.; Leger, L.; Tirrell, M. *Macromolecules* **1995**, *28*, 7419.
(28) Chen, Y.-L.; Helm, C. A.; Israelachvili, J. N. *J. Phys. Chem.* **1991**, *95*, 10736.
(29) Gent, A. N.; Schultz, J. *J. Adhes.* **1972**, *3*, 281.
(30) Andrews, E. H.; Kinloch, A. J. *Proc. R. Soc. London A* **1973**, *332*, 385.
(31) Ferry, J. D. *Viscoelastic Properties of Polymers*; Wiley: New York, 1980.
(32) Shanahan, M. E. R.; Carre, A. *Langmuir* **1995**, *11*, 1396.
(33) Klein, J. W.; Gnanou, Y.; Rempp, P. *Polym. Bull.* **1990**, *24*, 39.
(34) Hautekeer, J.-P.; Varshney, S. K.; Fayt, R.; Jacobs, C.; Jerome, R.; Teyssie, P. *Macromolecules* **1990**, *23*, 3893.
(35) Brandrup, J.; Immergut, E. H. *Polymer Handbook*; Wiley: New York, 1989.
(36) Hertz, H. In *Miscellaneous Papers*; Macmillan: London, 1896; p 146.
(37) Kline, S. J.; McClintock, F. A. *Mech. Eng.* **1953**, *75*, 3.
(38) Charlesby, A. *Proc. R. Soc. London A* **1954**, *222*, 542.
(39) Yoshizawa, H.; Chen, Y.-L.; Israelachvili, J. N. *J. Phys. Chem.* **1993**, *97*, 4128.
(40) Yoshizawa, H.; Chen, Y.-L.; Israelachvili, J. *Wear* **1993**, *168*, 161.
(41) Raphael, E.; de Gennes, P. G. *J. Phys. Chem.* **1992**, *96*, 4002.
(42) Brown, H. R. *Science* **1994**, *263*, 1411.
(43) Gent, A. N.; Petrich, R. P. *Proc. R. Soc. London A* **1969**, *310*, 433.
(44) Lim, W. W.; Mizumachi, H. *J. Appl. Polym. Sci.* **1995**, *57*, 55.
(45) Xu, D.-B.; Hui, C.-Y.; Kramer, E. J. *J. Appl. Phys.* **1992**, *72*, 3305.
(46) Cherry, B. W. *Polymer Surfaces*; Cambridge University Press: Cambridge, 1981.
(47) Barquins, M. *Wear* **1992**, *158*, 87.
(48) Sneddon, I. N. *Int. J. Eng. Sci.* **1965**, *3*, 47.
(49) Ganghoffer, J.-F.; Gent, A. N. *J. Adhes.* **1995**, *48*, 75.

MA9518924